Individuals, grasses, and forests of single- and multi-walled carbon nanotubes grown by supported Co catalysts of different nominal thicknesses

Kazunori Kakehi [a], Suguru Noda [a,*], Shigeo Maruyama [b], Yukio Yamaguchi [a]

[a] *Department of Chemical System Engineering, School of Engineering, The University of Tokyo, 7-3-1 Hongo, Bunkyo-ku, Tokyo 113-8656, Japan*

[b] *Department of Mechanical Engineering, School of Engineering, The University of Tokyo, 7-3-1 Hongo, Bunkyo-ku, Tokyo 113-8656, Japan*

Abstract

The relationships among the nominal thickness of Co catalyst, the structure of the catalyst particles, and the structure of carbon nanotubes (CNTs) growing from the catalyst during chemical vapor deposition were investigated. Various morphologies of CNTs such as individuals, random networks parallel to the surface of the substrate (‘grasses’), and vertically-aligned forests of single- and multi-walled carbon nanotubes were grown by only varying the nominal thickness of catalyst under the same reaction condition. These different morphologies at the same growth time were due to the different areal density rather than to the length of CNTs. With increasing nominal thickness of catalyst, the catalyst particles changed in diameter while their areal density remained relatively almost constant. The change in diameter possibly affected the number ratio of active catalyst particles to the whole particles, which in turn affected the areal density of CNTs and yielded the various morphologies. Longer growth time increased the CNT length, which caused further change in CNT morphologies from individuals to grasses and grasses to forests.

Keywords: single-walled carbon nanotubes; multi-walled carbon nanotubes; morphology; chemical vapor deposition; catalyst; combinatorial method

* Corresponding author. *E-mail address:* noda@chemsys.t.u-tokyo.ac.jp (S. Noda).

1. Introduction

Single-walled carbon nanotubes (SWCNTs) are nanomaterials that have attracted considerable attention for their application in nanodevices due to their unique properties [1], such as metallic or semiconductive conductivity depending on chirality, a high mechanical strength, and a large specific surface area. SWCNTs produced from catalysts on substrates have various morphologies such as individuals [2-5], random networks parallel to the surface of substrate (‘grasses’) [6-8], and vertically-aligned forests [9-15]. SWCNT individuals grown by reducing areal number density of SWCNTs is critical in nanodevices such as quantum wires [16] and chemical sensors [17], whereas vertically-aligned SWCNT forests are expected for applications such as optical devices [18] and capacitors [19]. Sparse or dense growth of SWCNTs has investigated separately, whereas comparison of these different morphologies is needed to further understand the mechanisms of such morphology evolution as well as to control SWCNT morphologies at higher degree.

The relationship between grass and vertically-aligned forests has been studied. For example, Zhang et al. investigated the effect of arrangement of Co-Mo bimetallic catalyst particles on the morphology of SWCNTs grown by chemical vapor deposition (CVD) from CO by varying the concentration of catalyst solution [13]. SWCNT grass or vertically-aligned SWCNTs were grown depending on the concentration of catalyst solution, and they proposed that the average distance between active particles, i.e. areal density of active particles plays an important role in determining the SWCNT morphology. Zhang et al. also found that SWCNTs in an individual bundle grow from a single alloy particle. Vertically-aligned growth of SWCNTs has also been intensively studied in alcohol catalytic CVD (ACCVD) [9, 20] and "supergrowth [10]", where a single SWCNT grows from a single particle [21, 22]. However, there are few reports on comparison of these different morphologies, and therefore, the underlying mechanism controlling the morphology of carbon nanotubes (CNTs) remains unknown.

By using the combinatorial method [23], we previously fabricated a gradient thickness

profile of catalyst and discovered that various types of CNTs grow depending on the amount of catalyst on substrate, i.e., its nominal thickness, which determines the diameter and areal density of the catalyst particles. For example, the morphology of SWCNTs (grasses or forests) was determined by the amount and composition of the Co-Mo bimetallic catalyst [24]. When a single element catalyst was used, i.e., Co catalyst, SWCNTs and multi-walled carbon nanotubes (MWCNTs) grew depending on the nominal thickness of catalyst, and a range of nominal thickness existed where neither SWCNTs nor MWCNTs efficiently grew [25].

Various types of CNTs can be grown by only varying the amount of catalyst even if the CVD conditions such as gas composition and CVD temperature are the same. In this study, we investigated in detail the relationships among the nominal thickness of catalyst, the structure of the catalyst particles, and the structure of the CNTs. Our experimental results suggest that CNT morphology, i.e., individuals, grasses and forests, depends on the difference in the areal density of growing CNTs, although the areal density of the catalyst nanoparticles remains relatively unchanged. Based on our results, we then discuss the different areal density of CNTs based on the diameter distribution of catalyst particles and the different catalytic activity among different-sized particles.

2. Experiment

The detailed procedures for catalyst preparation and CVD were described elsewhere [24-25]. Gradient thickness profiles of Co were prepared on Si substrates that had a thermal oxide layer. Catalysts were deposited on these substrates by sputtering with a mask. The mask was a 0.5-mm-thick metal sheet with a 2-mm-wide slit that was placed 3.6 mm above the substrate. Co was deposited at 1.3 Pa through the slit mask using a rf magnetron sputtering system with 2-inch targets. Although we used a batch-type sputtering system with a base pressure of ~10^{-4} Pa in previous research [25], we used a load-lock type sputtering system with a lower base pressure of ~10^{-6} Pa in this study. The gradient thickness profile of Co was obtained perpendicular to the slit,

with the nominal Co thickness (t_{Co}) ranging from 0.05 to 3.7 nm. For further observation of nanoparticles by transmission electron microscopy (TEM), we used high-temperature-tolerant TEM grids (Okenshoji microgrid NH type). TEM grids placed in a hot-wall quartz-glass tubular reactor were heated to 730 ˚C, and then tetraethylorthosilicate (TEOS) vapor was introduced into the reactor. By thermal decomposition of TEOS, TEM grids were coated by SiO_2. Co was uniformly deposited on the grids by sputtering without a mask. The samples on Si substrates and TEM grids were exposed to air and then placed in a hot-wall quartz-glass tubular reactor. The samples were heated to 700 ˚C under 5 vol% H_2/Ar flow at 2.7 kPa and kept at this temperature for 10 min. Then, for the sample on Si substrates, ACCVD was carried out by introducing pure ethanol vapor into the reactor at 1.3 kPa for 1, 3, and 10 min. The resulting samples were characterized by micro-Raman scattering spectroscopy (Seki Technotron STR-250) with an excitation wavelength of 488 nm, field-emission scanning electron microscopy (FE-SEM; Hitachi S-4700), and TEM (JEOL 2000EX).

3. Results and Discussion

Figure 1 shows photographs of samples after ACCVD. The nominal thickness profile of Co ranged from 0.05 nm (at left on sample) to 3.7 nm (right). For Regions I, II, III, and IV (indicated by arrows) located approximately 10, 6, 4.5, and 3.5 mm, respectively, from the right edge of the substrate, t_{Co} was 0.14, 0.21, 0.38, and 0.63 nm, respectively. Regions II and IV were dark in color, and increased in darkness with increasing time for ACCVD. Note that the right edge of the sample was colored by Co as thick as a few nanometers.

Figure 2 shows Raman spectra of the CNTs grown for Regions I-IV after ACCVD for 10 min. Similar tendency was observed between the color of the sample (Fig. 1) and these Raman spectra: The G-band was larger at the darker region. Although Regions I and III were not as dark as Regions II and IV, CNTs also grew in these regions. The peaks for the radial breathing mode (RBM) at low-wavenumber region (around 150-350 cm^{-1}) were more remarkable in Regions I and II,

indicating SWCNT growth in these regions. In contrast, the RBM peaks were weak in Regions III and IV, indicating mainly MWCNT growth. In our previous research [25], where Raman spectra and TEM images were correlated, similar results were obtained; SWCNTs and MWCNTs were mainly observed at t_{Co} = 0.13 and 1.5 nm, respectively. Two major differences exist between our previous research [25] and this study. First, the optimum t_{Co} for SWCNTs and MWCNTs (Regions II and IV) was 0.1 and 1.5 nm, respectively, in the previous research, and 0.2 and 0.6 nm in this study. Second, SWCNTs grew more efficiently in Region II, and CNT growth was not significantly suppressed in Region III. These differences were possibly due to the lower base pressure of the sputtering system (load-lock type) used in this current study compared with that (batch type) used in the previous study.

Figure 3 shows plan-view FE-SEM images of as-grown CNTs at different t_{Co}. At Region X with t_{Co} = 0.05 nm, (located approximately 14 mm from the right edge of the substrate as shown in Fig. 1), rather thick line patterns were observed at the initial stage of growth (Fig. 3a). This is a typical image of individual SWCNTs on an insulator [26]. After longer growth times of 3 and 10 min (Figs. 3b and c), the line patterns for Region X became thinner and networks of SWCNTs formed. Such increase in the amount of CNTs with time was also observed in the other regions as follows. In Region I, planar spaghetti-like bundles formed after 3 and 10 min. In Regions II-IV, CNT bundles appeared more sterically-bulky, suggesting the formation of 3D networks. CNTs in Region III were sparser than in Regions II and IV.

Figure 4 shows cross-sectional FE-SEM images of as-grown CNTs. At 1 min growth, CNT growth was confined on the 2D surface of the substrate for Regions I, III and IV, whereas it expanded to 3D space over the substrate surface for Region II. At 3 min growth, CNT growth was still confined on the 2D surface for Region I, whereas it expanded to 3D space as high as 0.7, 0.3, and 0.6 μm for Regions II, III and IV, respectively. Interestingly, CNTs had similar length of ~ 1 μm for 2D and 3D growth in Regions I and II, respectively.

Based on both the results of the Raman spectra (Fig. 2) and the SEM images (Figs. 3 and

4), the growth process can be summarized as follows. In Region X, growth of SWCNTs was sparse and formed individuals after 1 min growth but formed bundles and had a grass morphology after 3 min growth. In Region I, SWCNTs had a grass morphology after 1-3 min growth. In Region II, growth of SWCNTs was dense and formed a forest morphology after 1-3 min growth. In contrast, MWCNTs mainly grew in Regions III and IV and formed grass and forest morphologies after 1 and 3 min growth, respectively. Even at the same growth time of 1 min and only the nominal Co thickness was varied, SWCNTs had various morphologies, i.e., individuals, grasses, and forests in Regions X, I and II, respectively. Areal densities of SWCNTs clearly differed among those three conditions (Figs. 3a; Regions X, I, II), but the length was similar at about a half micrometer even for the individuals (Fig. 3a(X)) and the forest (Fig. 4a(II)). That is, the difference in the SWCNT morphology was caused by the difference in the areal density rather than the length of growing SWCNTs.

Figure 5 shows TEM images of Co particles and their diameter distribution of them based on number. At t_{Co} = 0.14, the average diameter was 2.8 ± 0.7 and the areal density was 1.1×10^4 , and at t_{Co} = 0.83 nm, they were 4.2 ± 1.0 nm and 1.3×10^4 / μm^2, respectively. For different nominal Co thicknesses at the subnanometer regime, the particles changed in size while the areal density remained relatively constant although it largely changed for thicker Co layers at nanometer regime [25].

In Regions X, I, II, the areal density of SWCNTs differed while the areal density of nanoparticles remained relatively unchanged. These contradicting results indicate that the activity ratio, defined as the number ratio of active catalyst particles to the whole particles [22], depended on the catalyst particle size. Because the SWCNT yield was the largest in Region II, Co particles should have had the highest activity ratio when their diameter was optimum at around 2.8 nm. The optimum diameter for the highest activity ratio will depend on the CVD condition [27]. The particle size decreased with decreasing nominal Co thickness, and the number ratio of optimally sized particles (i.e., around 2.8 nm in diameter) to the whole particles decreased, resulting in sparser

SWCNTs that formed morphologies of grasses (Region I) and individuals (Region X). This model explains the variety in morphologies of SWCNTs growing to a similar length at a different areal density from catalyst particles of similar density and different sizes. This can also explain the results for Regions III and IV; namely, the number ratio of active nanoparticles for the growth of MWCNTs was higher in Region IV than in Region III, and therefore, MWCNTs grew more densely in Region IV. The morphology of CNTs is not determined solely by their areal density, however. When the CNT length increased after 3 min growth, the morphology of the CNTs changed from individuals to grasses (Region X) and grasses to forests (Regions III and IV). Nominal CNT thickness, as the product of areal density, cross-sectional area, and length of CNTs, should therefore be an important index used to classify CNT morphologies. Further study is needed to establish this model.

4. Conclusions

The relationships among the nominal thickness of catalyst, the structure of the catalyst particles, and the structure of CNTs were investigated by applying combinatorial method to Co catalyst supported on SiO_2 surfaces. SWCNTs and MWCNTs of various morphologies, such as individuals, grasses and forests, were grown by only changing the nominal Co thickness under the same CVD conditions. SWCNTs had similar length, around a 0.5 μm, after 1 min growth time, and the resulting various morphologies were due to the difference in areal density of SWCNTs. Increase in the nominal thickness of the catalyst increased the catalyst particle size while the areal density of catalyst particles remained relatively constant at around 1×10^4 / μm^2. This contradiction between a different areal density of SWCNTs and a constant areal density of catalyst particles can be explained as follows. The activity ratio of catalyst depended on the catalyst particle size, which was optimum at a particle diameter of around 2.8 nm. The change in the activity ratio affected the areal density of the active catalyst, which in turn affected the areal density of growing SWCNTs. For a constant catalyst thickness, morphological change from individuals to grasses and from grasses to forests was also observed when the growth time was increased. Nominal CNT thickness is the

product of areal density, cross-sectional area, and length of CNTs, and should therefore be an important index used to classify CNT morphologies.

Acknowledgements

The authors thank Mr. H. Tsunakawa and Mr. T. Ito for assistance with the TEM, and Ms. Z. Zhang for assistance with the Raman measurements. This work was financially supported in part by a Grant-in-Aid for Young Scientists (A) #18686062 and Grant-in-Aid for Specific Research Area #19054003 by Ministry of Education, Culture, Sports, Science and Technology (MEXT), Japan. K. Kakehi was supported by the Global COE Program for Chemistry Innovation.

References

[1] R. Saito, G. Dresselhaus, M.S. Dresselhaus, Physical Properties of Carbon Nanotubes, Imperial College Press, 1998.

[2] J. Kong, H.T. Soh, A.M. Cassell, C.F. Quate, H. Dai, Nature 395 (1998) 878.

[3] Y. Li, W. Kim, Y. Zhang, M. Rolandi, D. Wang, H. Dai, J. Phys. Chem. B 105 (2001) 11424.

[4] A. Ismach, L. Segev, E. Wachtel, E. Joselevich, Angew. Chem. Int. Ed. 43 (2004) 6140.

[5] H. Ago, K. Nakamura, K. Ikeda, N. Uehara, N. Ishigami, M. Tsuji, Chem. Phys. Lett. 408 (2005) 433.

[6] L. Delzeit, B. Chen, A. Cassell, R. Stevens, C. Nguyen, M. Meyyappan, Chem. Phys. Lett. 348 (2001) 368.

[7] H. Hongo, M. Yudasaka, T. Ichihashi, F. Nihey, S. Iijima, Chem. Phys. Lett. 361 (2002) 349.

[8] Y. Murakami, Y. Miyauchi, S. Chiashi, S. Maruyama, Chem. Phys. Lett. 377 (2003) 49.

[9] Y. Murakami, S. Chiashi, Y. Miyauchi, M. Hu, M. Ogura, T. Okubo, S. Maruyama, Chem. Phys. Lett. 385 (2004) 298.

[10] K. Hata, D.N. Futaba, K. Mizuno, T. Namai, M. Yumura, S. Iijima, Science 306 (2004) 1362.

[11] G. Zhong, T. Iwasaki, K. Honda, Y. Furukawa, I. Ohdomari, H. Kawarada, Jpn. J. Appl. Phys. 44 (2005) 1558.

[12] G. Zhang, D. Mann, L. Zhang, A. Javey, Y. Li, E. Yenilmez, Q. Wang, J.P. McVittie, Y. Nishi, J. Gibbons, H. Dai, Proc. Natl. Acad. Sci. U.S.A. 102 (2005) 16141.

[13] L. Zhang, Y. Tan, D.E. Resasco, Chem. Phys. Lett. 422 (2006) 198.

[14] S. Noda, K. Hasegawa, H. Sugime, K. Kakehi, Z. Zhang, S. Maruyama, Y. Yamaguchi, Jpn. J. Appl. Phys. 46 (2007) L399.

[15] S. Oida, A. Sakai, O. Nakatsuka, M. Ogawa, S. Zaima, Appl. Surf. Sci, in press.

[16] S.J. Tans, M.H. Devoret, H. Dai, A. Thess, R.E. Smalley, L.J. Geerligs, C. Dekker, Nature 386 (1997) 474.

[17] J. Kong, N.R. Franklin, C. Zhou, M.G. Chapline, S. Peng, K. Cho, H. Dai, Science 287 (2000)

622.

[18] S. Yamashita, Y. Inoue, S. Maruyama, Y. Murakami, H. Yaguchi, T. Kotake, S.Y. Set, Jpn. J. Appl. Phys. 45 (2006) L17.

[19] D.N. Futaba, K. Hata, T. Yamada, T. Hiraoka, Y. Hayamizu, Y. Kakudate, O. Tanaike, H. Hatori, M. Yumura, S. Iijima, Nat. Mater. 5 (2006) 987.

[20] S. Maruyama, R. Kojima, Y. Miyauchi, S. Chiashi, M. Kohno, Chem. Phys. Lett. 360 (2002) 229.

[21] M. Hu, Y. Murakami, M. Ogura, S. Maruyama, T. Okubo, J. Catal. 225 (2004) 230.

[22] D.N. Futaba, K. Hata, T. Namai, T. Yamada, K. Mizuno, Y. Hayamizu, M. Yumura, S. Iijima, J. Phys. Chem. B 110 (2006) 8035.

[23] S. Noda, Y. Kajikawa, H. Komiyama, Appl. Surf. Sci. 225 (2004) 372.

[24] S. Noda, H. Sugime, T. Osawa, Y. Tsuji, S. Chiashi, Y. Murakami, S. Maruyama, Carbon 44 (2006) 1414.

[25] K. Kakehi, S. Noda, S. Maruyama, Y. Yamaguchi, Jpn. J. Appl. Phys. in press.

[26] Y. Homma, S. Suzuki, Y. Kobayashi, M. Nagase, D. Takagi, Appl. Phys. Lett. 84 (2004) 1750.

[27] C. Lu and J. Liu, J. Phys. Chem. B 110 (2006) 20254.

Figure captions

Fig. 1 Photograph of combinatorial samples after ACCVD for 1, 3, and 10 min.

Fig. 2 Raman spectra of CNTs after ACCVD for 10 min measured using 488-nm excitation. The intensity at the low-wavenumber region (< 350 cm^{-1}) is shown magnified by a factor 10.

Fig. 3 Plan-view FE-SEM images of as-grown CNTs with initial Co layers of different thicknesses: t_{Co} = 0.05, 0.14, 0.21, 0.38, and 0.63 nm (corresponding to Regions X, I, II, III and IV, respectively) after ACCVD for 1 (a), 3 (b), 10 min (c).

Fig. 4 Cross-sectional FE-SEM images of as-grown CNTs with initial Co layers of different thicknesses: t_{Co} = 0.14, 0.21, 0.38, and 0.63 nm (corresponding to Regions I-IV, respectively) after ACCVD for 1 (a) and 3 min (b).

Fig. 5 Plan-view TEM images of Co particles with uniform initial Co layers of thickness t_{Co} = 0.14 (a), 0.83 nm (b). (c) Distribution of the diameters of Co particles based on number obtained from TEM images.

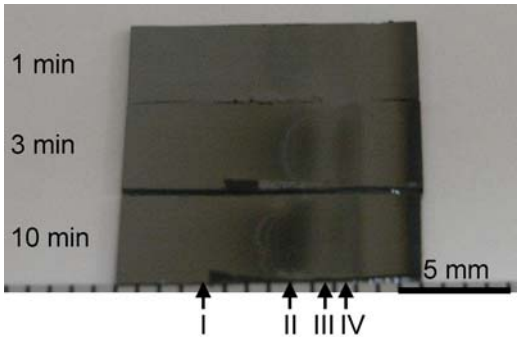
1 min
3 min
10 min
5 mm
I
II
III
IV

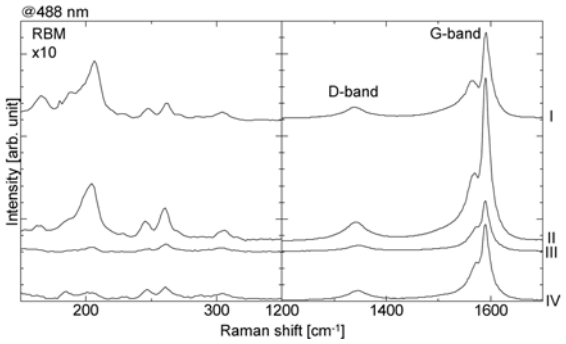
@488 nm
RBM
x10
G-band
D-band
I
II
III
IV
Intensity [arb. unit]
200
300
1200
1400
1600
Raman shift [cm-1]

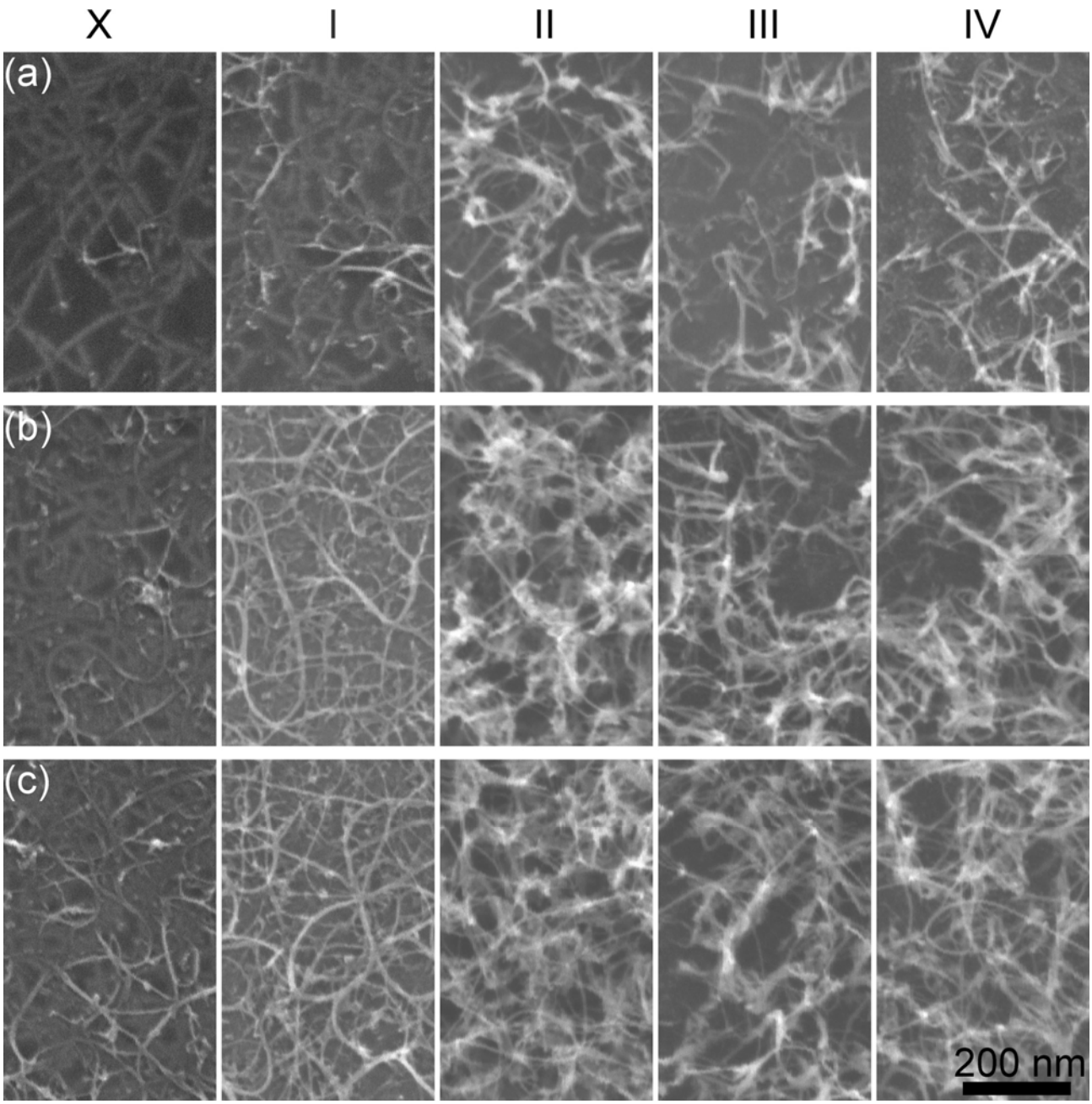
X
I
II
III
IV
(a)
(b)
(c)
200 nm

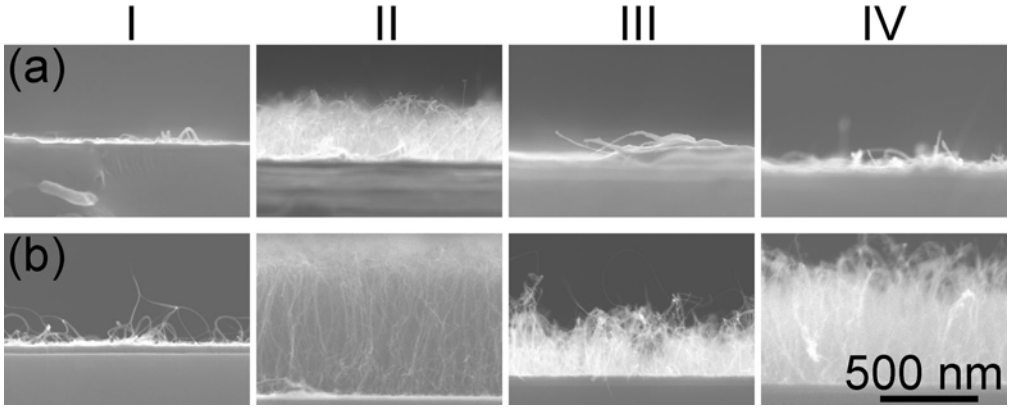
I
II
III
IV
(a)
(b)
500 nm

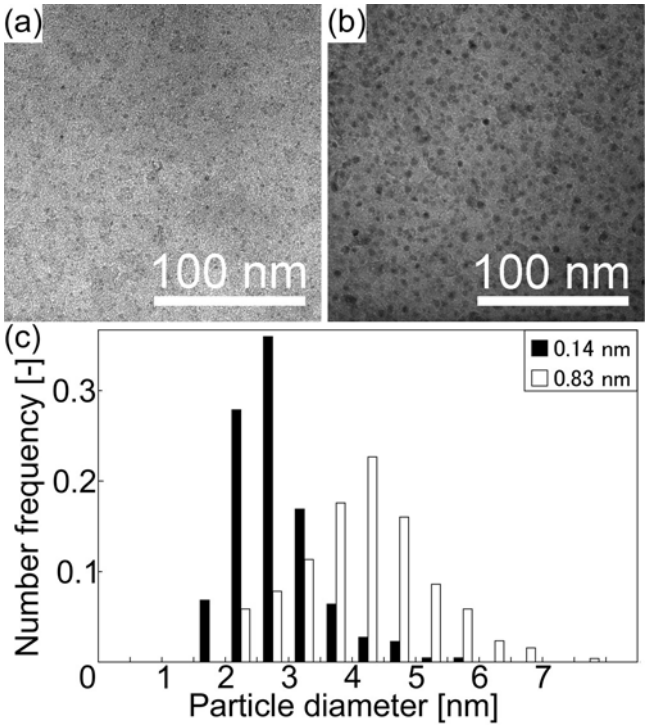
(a)
100 nm
(b)
100 nm
(c)
0.14 nm
0.83 nm
Number frequency [-]
0.3
0.2
0.1
0
1
2
3
4
5
6
7
Particle diameter [nm]